

# **Numerically Calculated Spherical Rayleigh–Taylor Growth Rates**

**Arun Thakar**

## Numerically calculated spherical Rayleigh-Taylor growth rates

Arun Thakar  
Advised by Reuben Epstein

Summer High School Research Program 2004  
Laboratory for Laser Energetics  
University of Rochester

### Abstract

In inertial confinement fusion, laser beams irradiate a spherical CH shell filled with deuterium-tritium gas, causing it to implode. The deceleration at the end of the implosion creates a Rayleigh-Taylor (RT) instability at the interface between the DT gas and the solid CH shell where small perturbations grow and quench the fusion reaction. Anderson and Betti have proposed reducing RT growth rates by altering the DT composition, thereby smoothing the density profile. Their estimated growth rates however, are inaccurate. A computer program for calculating RT growth rates was adapted to spherical geometry. Growth rates from this program and realistic density profiles confirm that the proposed technique is effective.

### I. Introduction

In inertial confinement fusion (ICF), laser beams irradiate a small spherical capsule, causing it to implode. The compression of the capsule during the implosion creates conditions for fusion, a reaction where deuterium (D) and tritium (T), two isotopes of hydrogen, collide and fuse, forming a larger Helium-4 atom as well as a neutron, thereby converting mass into kinetic energy. The spherical capsule, or “target”, consists of a thin plastic CH shell filled with DT. The targets used at the OMEGA laser, located at the Laboratory for Laser Energetics (LLE) of the University of Rochester, are approximately 1mm in diameter. The OMEGA laser is a 60-beam, 30-kJ, 351-nm wavelength laser used for direct-drive ICF<sup>1</sup>. The heat created by the compression of implosion on OMEGA—which can produce ion temperatures of 2 to 3 keV—

sustains the reaction.

In the first stage of ICF, called the acceleration phase, the initial heat of the absorbed laser pulse causes the CH shell to evaporate, or ablate. The pressure created by the ablation mimics rocket exhaust, forcing the target to implode. During the acceleration phase, there are three density regions: the hot ablating CH shell, the solid CH shell, and the cold DT core. After the laser pulse is complete, the target continues to converge as it enters the second phase called the coasting stage. In the third and final stage, the deceleration phase, the target reaches its maximum density and compression; fusion reactions occur in the core. Following the point of peak compression, the target bounces outwards, bringing an end to the process.

A major problem associated with ICF is the Rayleigh-Taylor instability.<sup>2</sup> When a fluid of lower density accelerates a fluid of higher density, the interface is said to be Rayleigh-Taylor unstable. The force applied to the system causes the initial imperfections, or perturbations, of an unstable interface to grow as an exponential function of time.

As seen in Fig.1, instability occurs within the plasma target at one of two interfaces. There is an outer location at the ablation surface—between the ablating CH shell and solid CH shell—and an inner location, at the fuel-shell interface—between the DT fuel and CH shell. The two instabilities do not occur simultaneously. Instability occurs at the exterior interface as the ablating CH shell drives the implosion during the acceleration phase and at the interior interface as the target compresses during the deceleration phase. Although both sites are important, this project focuses on the interior fuel-shell interface.

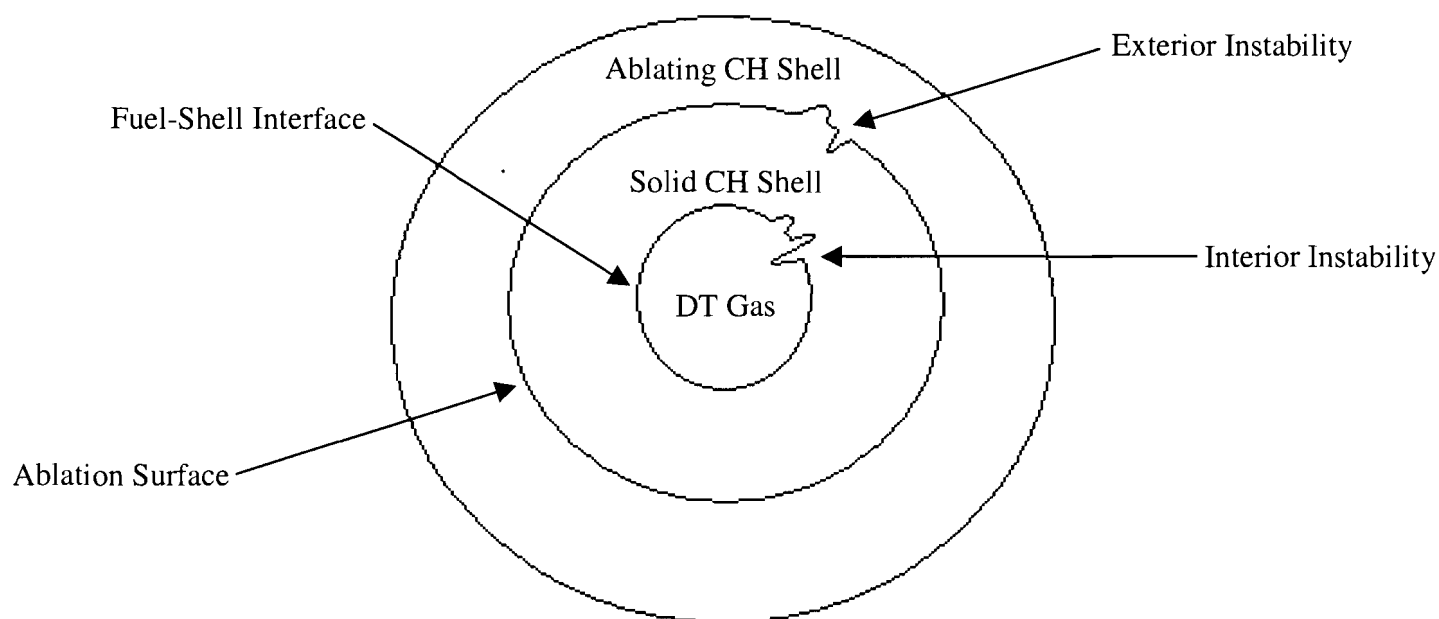


**Figure 1: A cross-section of an imploding target. The RT instability occurs at the interfaces between different layers of contrasting density.**

The sharp changes in density at the interfaces and the acceleration of the shell are what primarily determine the growth rate of the perturbations. The Rayleigh-Taylor instability is detrimental to the fusion reaction, because when the cooler shell dips into the hotter core, the shell quenches the process by drawing heat away from the fusion reactions. To reduce the growth rate of the instability, LLE scientists Kenneth Anderson and Ricardo Betti propose smoothing the density jump at the fuel-shell interface by altering the molecular composition of DT gas<sup>3</sup>, making it heavier, so there is a more gradual increase in density between the fuel core and the shell. The method they use to estimate the change in growth rate, however, does not take into account the realistically varying density profiles. A numerical method can provide a more reliable value for the growth rate than a simple estimate because it takes into account the whole density profile. Thus, the objectives of this project are to: (a) calculate Rayleigh-Taylor growth

rates in spherical geometry by using a numerical method that considers the details of the shell's density profile, and (b) apply this method to Anderson and Betti's density profiles to verify that their technique is effective.

## II. Finding a Rayleigh-Taylor Equation

The Rayleigh-Taylor instability is accurately modeled by a partial differential equation which expresses the instability in terms of the velocity of the perturbation, the growth rate of the perturbation, the acceleration of the system, and the density profile. S. Chandrasekhar presents such an equation<sup>4</sup> for a perturbation of an incompressible fluid that takes the form of a sinusoidal ripple along a perturbed planar surface. In the derivation of this equation  $v_i$ , ( $i=x,y,z$ ) represents the components of the velocity perturbation,  $\rho$  represents the unperturbed density,  $\delta\rho$  is the density perturbation,  $\delta p$  is the pressure perturbation, and  $g$  is the acceleration.  $\lambda_i$  denotes a unit vector in the  $z$  direction, the direction of the acceleration of magnitude  $g$ . We then know the following three equations:

$$\rho \frac{\partial v_i}{\partial t} = -\frac{\partial}{\partial x_i} \delta p - g \delta \rho \lambda_i, \quad (1)$$

$$\frac{\partial v_i}{\partial x_i} = 0, \quad (2)$$

and

$$\frac{\partial}{\partial t} \delta \rho + v_i \frac{\partial \rho}{\partial x_i} = 0. \quad (3)$$

Eq.1 is Newton's second law,  $F=ma$ , Eq.2 tells us that the fluid does not diverge, meaning that it does not spread. Finally, Eq.3 tells us that as we follow a fluid that does not diverge, its density

does not change. Eq.3 come from the conservation of mass. The next step is to rewrite Eq.1 in the x, y and z directions (*u, v and w*) separately:

$$\rho \frac{\partial u}{\partial t} = -\frac{\partial}{\partial x} \delta p, \quad (4)$$

$$\rho \frac{\partial v}{\partial t} = -\frac{\partial}{\partial y} \delta p, \quad (5)$$

and

$$\rho \frac{\partial w}{\partial t} = -\frac{\partial}{\partial z} \delta p - g \delta p. \quad (6)$$

Eq.2 states that the sum of the velocity gradients in the x, y and z directions must equal 0. This is mathematically expressed as:

$$\frac{\partial u}{\partial x} + \frac{\partial v}{\partial y} + \frac{\partial w}{\partial z} = 0. \quad (7)$$

Stipulating that the unperturbed density profile is a function of z only, we have:

$$\frac{\partial \rho}{\partial x} = \frac{\partial \rho}{\partial y} = 0, \quad (8)$$

and Eq.3 can be rewritten as:

$$\frac{\partial}{\partial t} \delta \rho = -w \frac{d\rho}{dz}. \quad (9)$$

Chandrasekhar assumes that the temporal and spatial dependence of the perturbation velocity and density are modeled by exponentials. This technique is called “separation of variables.” One advantage of this technique is that it is relatively easy to integrate and differentiate exponentials.

The equations are:

$$\delta \rho(\vec{x}, \vec{t}) = \delta \rho(z) e^{i(k_x x + k_y y)} e^{\eta}, \quad (10)$$

and

$$\delta\bar{v}(\bar{x}, \bar{t}) = \delta\bar{v}(z) e^{i(k_x x + k_y y)} e^{\gamma t}. \quad (11)$$

The wave number,  $k$ , is defined as  $2\pi/\lambda$  where  $\lambda$  is the wavelength and  $\gamma$  is defined as the dimensioned growth rate (in units of inverse time). If we take the derivatives with respect to  $t$ ,  $x$ ,  $y$  and  $z$  we can make some simplifications:

$$\frac{\partial}{\partial t} = \gamma, \frac{\partial}{\partial x} = -ik_x, \frac{\partial}{\partial y} = -ik_y, \text{ and } \frac{d}{dz} = D. \quad (12)$$

We can also say that:

$$u = \delta v_x, \quad v = \delta v_y, \text{ and } w = \delta v_z. \quad (13)$$

This changes Eq.4-7, and Eq.9 respectively into:

$$\rho\gamma u = -ik_x \delta p, \quad (14)$$

$$\rho\gamma v = -ik_y \delta p, \quad (15)$$

$$D\delta p = -\rho\gamma w - g\delta\rho, \quad (16)$$

$$ik_x u + ik_y v = -Dw, \quad (17)$$

and

$$\gamma\delta p = -wD\rho. \quad (18)$$

Next, Chandrasekhar multiplies Eq.14 and 15 by  $ik_x$  and  $ik_y$  respectively and adds the products together, yielding:

$$(k_x^2 + k_y^2)\delta p = \rho\gamma(ik_x u + ik_y v). \quad (19)$$

Substituting Eq.17 and 18 into Eq.19 produces:

$$k^2 \delta p = -\gamma\rho Dw, \quad (20)$$

where  $k^2$  is defined as:

$$k^2 = k_x^2 + k_y^2. \quad (21)$$

In order to eliminate the pressure perturbation we will need one more equation, obtained by substituting Eq.18 into Eq.16:

$$D\delta p = -n\rho w + \frac{g}{\gamma} w D\rho. \quad (22)$$

Chandrasekhar eliminates  $\delta p$  using Eq.20 and Eq.22, producing a differential equation for the perturbation velocity in planar geometry:

$$\frac{d}{dz} \left[ \rho \frac{dw}{dz} \right] - \rho k^2 w + \frac{k^2 g}{\gamma^2} \left[ \frac{d\rho}{dz} \right] w = 0. \quad (23)$$

This equation assumes no surface tension and no viscosity. In the equation,  $\gamma^2/kg$  is a dimensionless squared growth rate of the perturbations, where  $\gamma$  is the dimensioned growth rate. Dimensionless quantities are used because they allow the simplification of complex mathematical expressions in computer code. Also, seeking the dimensionless quantities of a problem reveals the characteristic scales, such as time,  $(kg)^{-1/2}$ , and distance,  $k^{-1}$ .

To find an analytic solution to Eq.23, we need a sample case. For a simple step density jump, where  $\rho_2$  is greater than  $\rho_1$ , the dimensionless squared growth rate is equal to the Atwood number

$$\frac{\gamma^2}{kg} = A \quad (24)$$

defined as:

$$A = \frac{(\rho_2 - \rho_1)}{(\rho_2 + \rho_1)}. \quad (25)$$

Anderson and Betti used the Atwood number to gauge the effectiveness of their proposed smoothing technique. The formula assumes that there is a discontinuity in the density profile and that the rest of the density along the profile is constant. However, the density profiles that

Anderson and Betti consider are continuously variable, not simple in shape. Therefore the Atwood number's use in the situation is likely to be a poor approximation of the true dimensionless squared growth rate.

To investigate how one finds an analytic solution to the differential equation, I solved Eq.22 for a square-wave density profile. The square wave creates a second interface from which instability can arise, as well as a third density region,  $\rho_3$ . However, for simplicity, we assume that  $\rho_3$  is equal to  $\rho_1$ .

Figure 2 illustrates the square-wave problem. The function which peaks on the left is the perturbation velocity, and the square wave is the density profile. The  $z$  labels will be used later to explain the analytic solution for the equation.

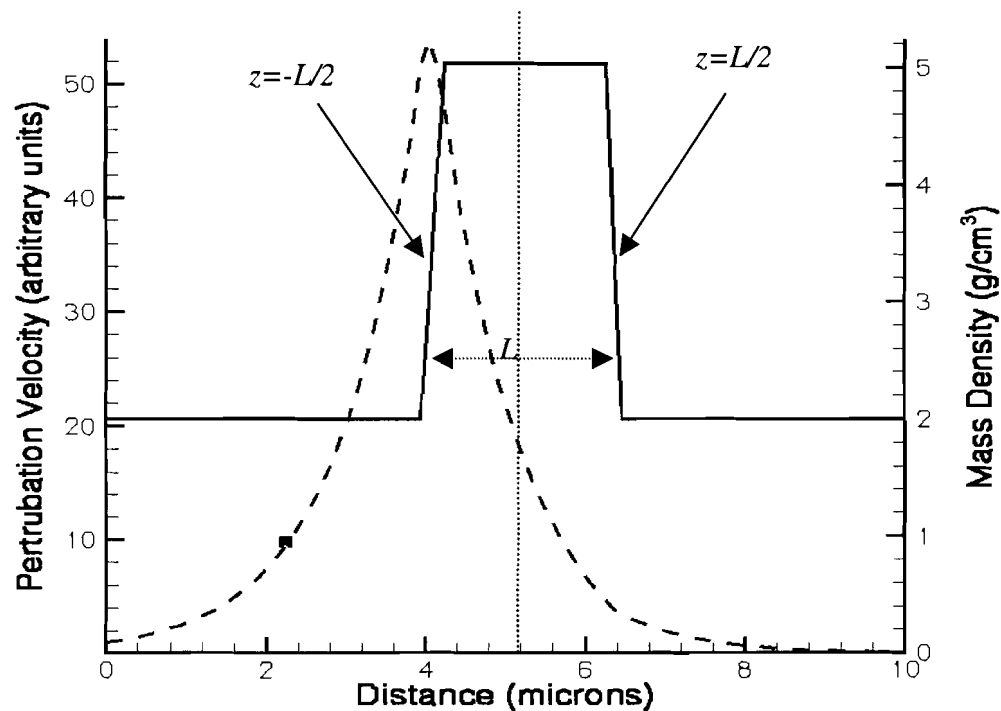


**Figure 2:** The solid line represents the density profile of the shell, and the dashed line represents the perturbation velocity. The perturbation velocity peaks at the first interface.

The type of differential equation we are solving is called an eigenvalue equation.

The set of solutions to eigenvalue equations is a set of eigenfunctions each with a corresponding eigenvalue. In this case,  $w(z)$ , the velocity perturbation is the eigenfunction, and  $\gamma^2/kg$ , the dimensionless squared growth rate, is the eigenvalue. To solve the differential equation and obtain the eigenfunction, one must integrate it and apply matching and boundary conditions, which depend on the chosen case.

How we expect the function to act as it goes to negative and positive infinity are the boundary conditions. We know the solution to the differential equation over the different constant regions of the density profile. Logically, the perturbation speed cannot be growing infinitely large when we are very far from the interface. The boundary conditions state that the velocity perturbation must approach zero as we travel away from the density jump. Assuming that

$$\frac{\partial \rho}{\partial z} = 0, \quad (26)$$

within the constant density regions. The solution to the differential equation for the first region,  $\rho_1$ , is:

$$w_1 = Ae^{kz}, \quad (27)$$

for the second region,  $\rho_2$ , is:

$$w_2 = Be^{kz} + Ce^{-kz}, \quad (28)$$

and for region,  $\rho_3$ , is:

$$w_3 = De^{-kz}. \quad (29)$$

The matching conditions are found at the interfaces where two perturbation velocity equations come into contact. Because the velocities of Eqs.27 and 28 are continuous at the first peak in Figure 2, we know that Eqs.27 and 28 give equal values for the perturbation at  $z = -L/2$ .

Using this information we get:

$$A = B + Ce^{kL}. \quad (30)$$

The other matching condition is at the second density discontinuity at  $z=L/2$  where Eqs.28 and 29 are continuous. The equation we get from this is:

$$D = Be^{kL} + C. \quad (31)$$

An expression for the dimensionless growth rate can be found much the same way as in the single-jump case. We integrate Eq.23 over the first density discontinuity, getting:

$$\rho_2 \frac{dw_2}{dz} - \rho_1 \frac{dw_1}{dz} + \frac{gk^2}{\gamma^2} (\rho_2 - \rho_1) w_1 = 0. \quad (32)$$

Doing the same over the second density discontinuity yields:

$$\rho_3 \frac{dw_3}{dz} - \rho_2 \frac{dw_2}{dz} + \frac{gk^2}{\gamma^2} (\rho_3 - \rho_2) w_2 = 0. \quad (33)$$

After allowing  $\rho_1 = \rho_3$ , we have enough information to solve for the dimensionless growth rate, expressed as:

$$\frac{\gamma^4}{k^2 g^2} = \frac{(e^{2kL} - 1)(\rho_2 - \rho_1)^2}{e^{2kL} \cdot (\rho_2 + \rho_1)^2 - (\rho_2 - \rho_1)^2}. \quad (34)$$

$\gamma^4/k^2 g^2$  is the square of the squared growth rate quantity, which is what we are trying to find, the heavy fluid mass density is  $\rho_2$  and the light fluid mass density is  $\rho_1$ ,  $g$  is the acceleration of the implosion, and  $L$  is the thickness of the shell. Because the product  $kL$  is dimensionless, we are expressing the thickness of the shell in units of the wavelength. This makes  $kL$  more significant than just  $L$ . I verified the analytic solution using Jue Liao's program<sup>5</sup>, which calculates the dimensionless growth rate of the perturbation velocities in the planar geometry when given a shell length,  $L$ , and a density profile.

If we evaluate Eq.34 for the limit of  $kL$  approaching infinity, the dimensionless

squared growth rate,  $\gamma^2/kg$ , becomes the Atwood number, the rate given by Eq. 24 for a single interface. In this limit where a large number of wavelengths separate the two interfaces, the perturbations act independently as they do at single-step interfaces. They are isolated and do not influence each other.

### III. A Rayleigh-Taylor equation in spherical geometry

The next step was to write a program that calculates Rayleigh-Taylor growth rates in spherical geometry. To do this I needed a differential equation for the velocity perturbation in spherical geometry. Dr. Epstein assisted me by deriving the equation<sup>6</sup>, which is:

$$\frac{l(l+1)}{x^2} \left[ 1 - \frac{g}{\gamma_0^2 \cdot R_0} \frac{1}{\rho} \frac{d\rho}{dx} \right] \cdot y - \frac{1}{\rho} \frac{\partial}{\partial x} \left[ \rho \frac{\partial y}{\partial x} \right] = 0. \quad (35)$$

There are striking similarities between this spherical equation and the planar Eq.23, with the wave number  $k$  replaced by  $l/R_0$ .  $l$  is called the modal index and  $R_0$  is the radius of the target at the instant where the shell is momentarily static, or at the “bounce.” The change in  $k$  makes the new dimensionless squared growth rate  $\gamma_0^2 R_0/g$  found inverted in the formula. The perturbation function is expressed as  $y$ , which is defined as  $y=wr^2$  where  $w$  is the perturbation velocity and  $r$  is the radial coordinate. The shell radius is made dimensionless by letting  $x=r/R_0$ . Finally, the  $(l+1)$  term arises due to properties of spherical harmonics. Harmonic functions such as those we use to model the perturbations behave differently in spherical geometry than sine and cosine do in planar geometry in subtle but important ways.

Another significant difference between Eq.35 and 23 is that the boundary conditions in the spherical case are now expressed as a power law and no longer exponential functions. The solution to Eq.35, assuming constant density, is for a radius,  $r$  near  $r=0$ :

$$y = x^{l+1} \quad (36)$$

and for a radius,  $r$  far greater than  $R_0$ ,

$$y = x^{-l} . \quad (37)$$

We see that Eqs.36 and 37 satisfy the boundary conditions requiring that the inner and outer velocity perturbations be equal to zero. This is similar to the boundary conditions in planar geometry, except that the inner boundary condition now applies at  $r=0$  rather than at  $z=-\infty$ .

#### **IV. Adapting an existing program to function in the spherical geometry**

Next, I adapted Jue Liao's program to function in spherical geometry. To do this, equations in the program used to solve Eq.23 were reworked to solve Eq.35. In spherical geometry, the user must enter  $R_0$  and  $l$  instead of  $kL$ . Also, the program allows the user to enter an arbitrary density profile, by importing it through a data file. This is a significant improvement over the old program where the user entered simple density profiles by hand.

The numerical method used by the program to determine the growth rate is called the "shooting method". The shooting method works as follows: The user enters an initial guess for the growth rate (eigenvalue) into the program, and the perturbation velocity is calculated for the whole density profile by integrating Eq.35 from  $r=0$  to the end of the density profile. We are shooting for a perturbation velocity of zero as  $r$  approaches infinity. If the boundary condition is not satisfied, the guess of the growth rate is adjusted based whether or not the perturbation velocity was overestimated or underestimated at the right boundary, and the perturbation velocity is recalculated for the entire density profile. The iteration process continues until the program converges on the growth rate which allows the perturbation velocity to satisfy the boundary conditions. When the perturbation velocity satisfies the boundary condition, the dimensionless squared growth rate is the eigenvalue, and the perturbation velocity is the eigenfunction.

In order to input the equation into the computer, one must split the second-order differential equation into two first-order differential equations. The equation becomes easier to work with once some substitutions are made:

$$\Gamma = \frac{\gamma_0^2 R_0}{g} \text{ and } A = \frac{1}{\rho} \frac{d\rho}{dx}. \quad (38)$$

The dimensionless squared growth rate will now be referred to as  $\Gamma$ . Entering these substitutions into Eq.35 yields:

$$\frac{l(l+1)}{x^2} \left[ 1 - \frac{A}{\Gamma} \right] y - \frac{1}{\rho} \frac{\partial}{\partial x} \left[ \rho \frac{\partial y}{\partial x} \right] = 0. \quad (39)$$

Next, we can carry out the indicated differentiation on the second term, making the equation:

$$\frac{l(l+1)}{x^2} \left[ 1 - \frac{A}{\Gamma} \right] y - \frac{1}{\rho} \frac{\partial \rho}{\partial x} \frac{\partial y}{\partial x} - \frac{\partial^2 y}{\partial x^2} = 0. \quad (40)$$

This creates another  $A$  term making the equation:

$$\frac{l(l+1)}{x^2} \left[ 1 - \frac{A}{\Gamma} \right] y - A \frac{\partial y}{\partial x} - \frac{\partial^2 y}{\partial x^2} = 0. \quad (41)$$

One more substitution will greatly simplify the equation before the final split:

$$B = \frac{l(l+1)}{x^2} \left[ 1 - \frac{A}{\Gamma} \right]. \quad (42)$$

Now the equations can be split by defining:

$$v = \frac{\partial y}{\partial x} \text{ and therefore } \frac{\partial^2 y}{\partial x^2} = \frac{\partial v}{\partial x}. \quad (43)$$

This results in two first-order differential equations:

$$\frac{\partial y}{\partial x} = v \text{ and } \frac{\partial v}{\partial x} = Bv - Av. \quad (44)$$

To convert these equations into a form suitable for entry in a programming

language, FORTRAN in my case, I needed to write these as simple step equations. Numerical methods utilize step equations, which calculate values for  $y$  and  $v$  at each iteration. In the program  $J$  denotes which spatial point the program has calculated last. As the program creates the whole integration grid,  $J$  increases until it reaches its final value (specified by the user). The step equations are centered half-way between each integration point:

$$\frac{y_{J+1} - y_J}{x_{J+1} - x_J} = \frac{v_{J+1} - v_J}{2} \quad (45)$$

and

$$\frac{v_{J+1} - v_J}{x_{J+1} - x_J} = B \left( \frac{y_{J+1} + y_J}{2} \right) - A \left( \frac{v_{J+1} + v_J}{2} \right). \quad (46)$$

Making the substitution

$$H = \frac{x_{J+1} - x_J}{2} \quad (47)$$

into Eqs. (45) and (46) and solving the two equations simultaneously, we obtain the step equations used in the FORTRAN program:

$$y_{J+1} = \frac{(H^2 B + HA + 1)y_J + 2Hv_J}{(-H^2 B + HA + 1)} \quad (48)$$

and

$$v_{J+1} = \frac{2HB y_J + (H^2 B - HA + 1)v_J}{(-H^2 B + HA + 1)}. \quad (49)$$

## V. Application of the program to proposed density profiles

The next step was to apply the working program to realistically important density

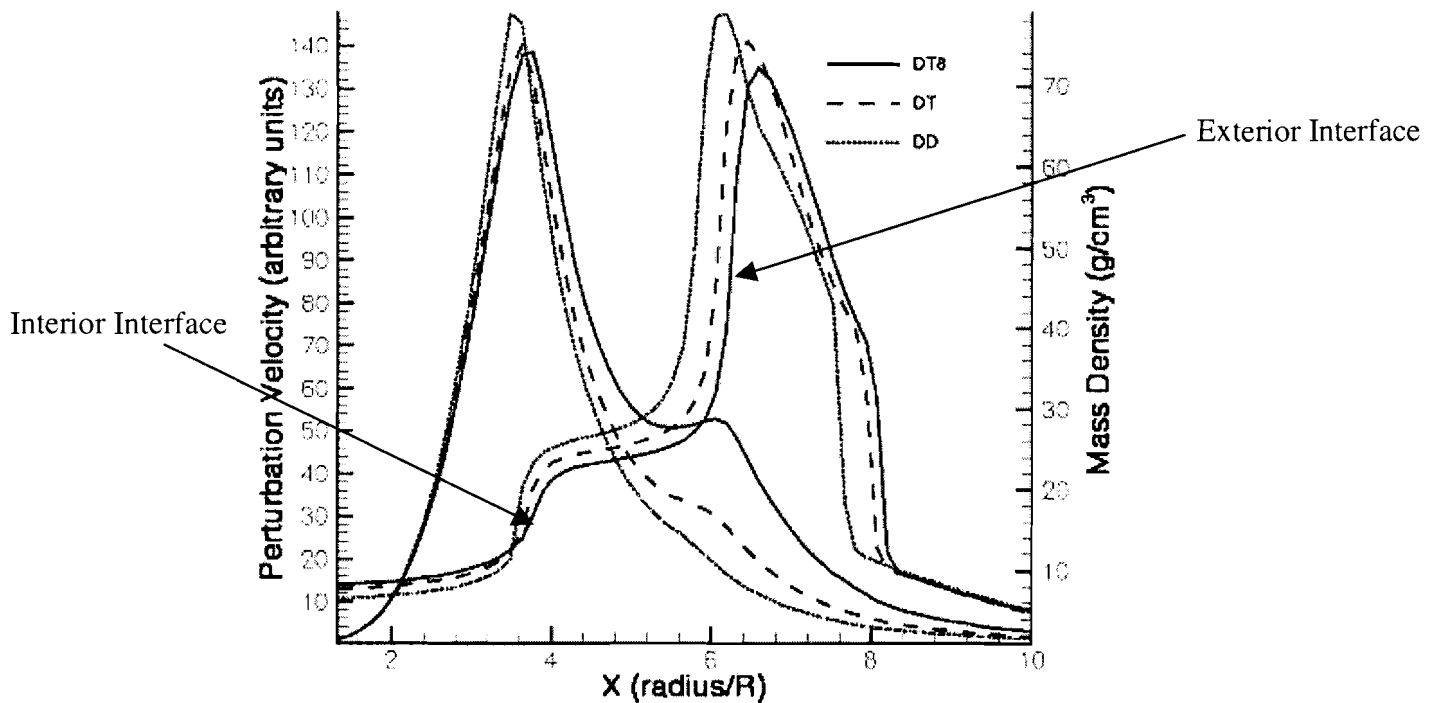
profiles. Kenneth Anderson and Ricardo Betti simulated density profiles where the fuel-shell density jump is smoothed out in order to reduce the growth rate of the instability. They did this by altering the composition of deuterium-tritium gas proportions of the fuel in hydrodynamic simulations of OMEGA implosions. As stated earlier, the Atwood number is not an accurate estimate because it is defined for a single interface separating fluids of constant density, which is not a good description of the density profile of the shell of an ICF implosion near peak compression. The numerical program can find a growth rate in spherical geometry for the proposed density profile.

Figure 3 below shows a graph of the perturbation velocities calculated by the program, as well as three corresponding density profiles that Anderson and Betti used. The density profiles are functions that peak on the right, and the perturbation velocities are the functions that peak on the left. Each line corresponds to a different composition of DT gas. The solid line is the altered  $DT_8$  gas that creates a smoothed density profile. The ratio of tritium molecules to deuterium molecules is eight to one. Since more of the heavy molecule is used, the mass density increases, accounting for the smoothing effect. The dashed line represents the density obtained using standard DT gas as the fill gas, and the dotted line is obtained using DD gas. The program gives us values for the dimensionless growth rates which we can convert back to dimensional units. We assume there are 100 points of spatial integration, and the  $l$  mode index value is 5; making the wavelength  $\lambda=56.5 \mu\text{m}$  for  $R_0=45\mu\text{m}$ . 100 points of integration insures that the shape of the eigenfunction will be resolved without creating unnecessary steps, while still accurately describing the eigenfunction's form. The value for  $R_0=45\mu\text{m}$  is chosen because it is the radius at which the fuel-shell interface is located at peak compression. The dimensionless squared growth rate ( $\Gamma$ ) produced by the program for  $DT_8$  is 0.65. The

dimensionless squared growth rates for standard DT and DD are  $\Gamma = 0.75$  and  $0.81$ , respectively. Anderson and Betti's estimates using the Atwood number are as follows:  $\Gamma = 0.0$  for DT<sub>8</sub>,  $0.26$ - $0.33$  for standard DT and  $0.43$ - $0.47$  for DD gas. It is clear that the numerical solution has provided a better estimate of the instability's growth rate and makes an important correction.

We also have enough evidence to state that even for low  $l$  mode values, smoothing the density ramp by altering the composition of the DT gas reduces the growth rate of the Rayleigh-Taylor instability. It is important to note that an infinite number of possible eigenfunctions for smaller values of  $\Gamma$  exist; we are primarily interested, however, in the function with the highest eigenvalue. For instance, the program produces an eigenfunction with a lower growth rate. This function dips far below the x-axis before returning up to meet the right boundary condition.

The perturbation velocity in Fig.3 is expressed in terms of "arbitrary units" because changing the normalization of the eigenfunctions by a constant factor does not affect the growth rates. One can multiply any of the eigenfunctions by constants and the calculated growth rates will remain the same.



**Figure 3: The three representative density profiles peak on the right, while the perturbation velocity profiles peak on the left. The smoothed DT8 density profile produces the lowest peak of the three meaning that the perturbation velocity and the instability is the lowest of the three.**

## VI. Conclusions

The spherical Rayleigh-Taylor program is a useful tool that can be used to see the impact of altering the density profile on the growth rate of the Rayleigh-Taylor instability. In addition to this primary purpose, the program also provides the perturbation velocity across the whole density profile. The results show us a variety of interesting features of the perturbation velocities: First, the velocity perturbation is significantly larger at the fuel-shell interface than the ablation surface. This is interesting because the second density jump, the one located at the ablation surface, is far greater than the one at the fuel-shell interface. Intuitively, one would expect the more conspicuous features of the density profile to have a greater effect on the perturbation velocity; however, this is not so. This verifies that the instability is greatest at the fuel-shell interface at peak compression. As we move to higher  $l$  values, the second peak will

become better defined. This is because the wavelength of the velocity perturbations at high  $l$  values is very small; accordingly the interaction between the perturbations is less. Another interesting result is that the smooth DT<sub>8</sub> profile has a significantly larger second velocity perturbation peak, relative to the DT and DD gases.

A problem with the program is that the step equations are “stiff”, which makes it difficult for the program to function with high  $l$  mode values. The step equations used in the program are very sensitive at high  $l$  values, meaning that results vary greatly with minor changes in input. If the program is given a guess that is slightly too high or too low it will not give the eigenfunction with the highest eigenvalue, the one we seek. In the future, it would be beneficial to apply the program to high  $l$  mode values. This can give us even more information about the perturbation velocity and the growth rate. At this stage of development, however, the program still serves as a valuable tool because it more accurately calculates RT growth rates for arbitrary density profiles in spherical geometry than previous approximate methods.

## **VII. Acknowledgements**

I would like to thank my advisor Dr. Reuben Epstein for helping me through my project. I would also like to thank Dr. Ricardo Betti and Mr. Kenneth Anderson for providing me density profiles which I could use for my project, as well as Dr. Stephen Craxton and the Laboratory of Laser Energetics for running such an excellent program. Finally I would like to thank all of the high school participants who made the summer a phenomenal experience.

## **VIII. References**

1. "A Unique Natural Resource." Laboratory for Laser Energetics. 1 November 2004.  
<[http://www.lle.rochester.edu/02\\_visitors/02\\_aboutomega.html](http://www.lle.rochester.edu/02_visitors/02_aboutomega.html) >.
2. G. Taylor, Proc. R. Soc. London Ser. A **201**, 192 (1950).
3. K. Anderson and R. Betti, private communication.
4. S. Chandrasekhar. *Hydrodynamic and Hydromagnetic Stability*. International Series of Monographs on Physics (Dover Publications, Inc., New York, 1961), Chap. X, p. 428.
5. Jue Liao. "Rayleigh-Taylor growth rate for arbitrary density profiles calculated with a variational method." Laboratory for Laser Energetics Summer High School Project Report. 2002.
6. R. Epstein, private communication.